Supplementary Information

Ascorbic Acid–Mediated Solid-State Synthesis of Cavity-Engineered CuO–Cu_2O–Cu Heterostructures: Structural Transformation Mechanism and Photocatalytic Detoxification of Cr(VI)

Mona S. NourEldien[1*], Mostafa Y. Nassar[2*]

[1]Department of Chemistry, Faculty of Science, Benha University, Benha 13518, Egypt

[2]Department of Chemistry, College of Science, King Faisal University, Al-Ahsa 31982, Saudi Arabia

[*]**Corresponding authors.**

E-mail address: mona.noureldin@fsc.bu.edu.eg, Tel: +20 01129618280 (M.S.N.).
Email address: mynassar@kfu.edu.sa. Tel: 00966538871438 (M.Y.N.).

S1. Characterization of CuO–Cu_2O–Cu Heterostructures

Samples were characterized as follows; X-ray diffraction (XRD): Bruker D8 Advance, Cu Kα (λ = 1.5406 Å), 2θ range 10°–80°, step size 0.02°, counting time 1 s/step. Phase identification used JCPDS cards; crystallite sizes were estimated from FWHM of selected peaks using the Scherrer equation $D = \frac{K\lambda}{\beta cos\theta}$ with K = 0.9. Reported β values were corrected for instrumental broadening using a Si standard. Fourier transform infrared (FT-IR): Thermo Nicolet iS10, 4000–400 cm^{-1}, 4 cm^{-1} resolution, 32 scans, KBr pellet method. Assignments follow references cited in the text. X-ray photoelectron spectroscopy (XPS): Thermo Fisher with Al Kα radiation (hν = 1486.6 eV, resolution ~ 0.5 eV at pass energy 20 eV). Survey spectra were collected in the - 10 to 1350 eV rangespot size 400 μm, at a pressure of 10 mbar with a full spectrum pass energy of 200 eV and at a narrow spectrum of 50 eV. A low-energy electron flood gun was used for charge neutralization during acquisition, and binding energies were calibrated with respect to the C 1s peak at 284.8 eV. Relative atomic concentrations and oxidation states are reported. FE-SEM and EDX: Quanta 250 FEG at 5–15 kV for morphology and elemental mapping. HR-TEM & SAED: JEOL JEM-2100 at 200 kV. Sample preparation used ethanol dispersion on lacey carbon grids. N_2 adsorption/desorption isotherms at 77 K were employed to examine the textural surface characteristics and pore size distribution using a BELSORP36 analyzer (JP. BEL Co., Ltd). UV–vis diffuse reflectance spectroscopy (DRS): Jasco V-670 with integrating sphere, $BaSO_4$ reference. Reflectance R(λ) converted to Kubelka–Munk function F(R) for Tauc analysis. Tauc plots were constructed using $(F(R)h\nu)^n$ Versus $h\nu$. Electron paramagnetic resonance (EPR) measurements were performed on a Bruker EMXPLUS spectrometer. The point of zero charge (pH_pzc) of the CuO–A1.1 catalyst was determined using the pH drift method. Briefly, a series of NaCl aqueous solutions (0.01 M) were prepared, and their initial pH values (pH_i) were adjusted in the range of 2–10 using dilute HCl or NaOH. A fixed amount of catalyst (0.01 g) was then added to each solution, and the suspensions were stirred and allowed to equilibrate at room temperature for 24 h. The final pH values (pH_f) were measured, and the pH_pzc was determined from the intersection point where ΔpH equals zero.

S2. Electrochemical Impedance Spectroscopy Measurements

EIS measurements were conducted using an electrochemical analyzer (model: CHI608D, CH Instruments, Austin, USA) over 100 Hz–300 kHz to probe the electrical properties of the samples. Pellets coated with conductive electrodes were used to ensure good contact. The real

(Z′) and imaginary (Z") impedance components, along with the phase angle, were analyzed to evaluate resistive and capacitive behavior and assess interfacial charge-transfer efficiency.

S3 Experimental and Statistical Analysis

All experimental runs were conducted in triplicate (n=3) under each tested condition, and the results are presented as the mean ± standard deviation (SD). Statistical analyses were performed using OriginPro 2019b (OriginLab Corporation, USA). For each experimental factor (solution concentration, pH, and catalyst dosage), descriptive statistics were first calculated to determine the mean, standard deviation, and standard error. The effects of these factors on Cr(VI) photoreduction efficiency were evaluated using one-way analysis of variance (ANOVA) at a 95% confidence level. Levene's test was used to verify homogeneity of variances, and Tukey's honest significant difference (HSD) test was used for post hoc pairwise comparisons among the treatment levels. Statistical significance was considered at $p < 0.05$. The use of one-way ANOVA was appropriate since each one-factor-at-a-time (OFAT) experiment involved varying a single factor at multiple levels while keeping all other conditions constant. For kinetic analysis, time-dependent concentration data (C_t/C_0 vs. time) obtained from the batch photoreduction experiments were also analyzed in OriginPro 2019b. Each time-point measurement was conducted in triplicate, and the mean ± SD values were used to generate kinetic plots. The pseudo-first-order kinetic model was fitted to the data by linear regression of $\ln(C_t/C_0)$ versus time, and the apparent rate constant (k, min^{-1}) and coefficient of determination (R^2) were obtained automatically from the regression statistics. The goodness of fit and reproducibility of the kinetic data were confirmed by the high R^2 values and small standard deviations among replicates. The combination of OFAT experimental design, replicate data collection, and integrated statistical evaluation using ANOVA, Levene's, and Tukey's tests provided a robust and reproducible statistical validation of the results. The inclusion of all raw replicate data in Table S3 ensures transparency and reproducibility of the statistical results presented.

Table S1. List of Abbreviations and Symbols

Term / Symbol	Definition / Meaning
Cr(VI)	Hexavalent Chromium
Cr(III)	Trivalent Chromium
CuO	Copper(II) Oxide
Cu_2O	Copper(I) Oxide / Cuprous Oxide
Cu	Metallic Copper
CuO–A0.2	CuO reduced with 0.2 g ascorbic acid
CuO–A0.5	CuO reduced with 0.5 g ascorbic acid
CuO–A0.8	CuO reduced with 0.8 g ascorbic acid
CuO–A1.1	CuO reduced with 1.1 g ascorbic acid (optimized sample)
FESEM	Field Emission Scanning Electron Microscopy
HRTEM	High-Resolution Transmission Electron Microscopy
XPS	X-ray Photoelectron Spectroscopy
OFAT	One-Factor-at-a-Time
ANOVA	Analysis of Variance
R^2	Coefficient of Determination
XRD	X-ray Diffraction
FTIR	Fourier Transform Infrared Spectroscopy
SEM	Scanning Electron Microscopy
TEM	Transmission Electron Microscopy
UV–Vis DRS	Ultraviolet–Visible Diffuse Reflectance Spectroscopy
EPR	Electron Paramagnetic Resonance

Term / Symbol	Definition / Meaning
EIS	Electrochemical Impedance Spectroscopy
R_{ct}	Charge Transfer Resistance
AA	Ascorbic Acid
DPC	1,5-Diphenylcarbazide
DI water	Deionized Water
JCPDS	Joint Committee on Powder Diffraction Standards
FWHM	Full Width at Half Maximum (β)
λ	Wavelength
θ	Bragg Angle
TG–FTIR	Thermogravimetric–Fourier Transform Infrared Spectroscopy
EDX	Energy-Dispersive X-ray Spectroscopy
SAED	Selected Area Electron Diffraction
k	Pseudo-First-Order Rate Constant
IPA	Isopropanol
BQ	Benzoquinone
$\cdot O^{2-}$	Superoxide Radical
e^-	Electron
h^+	Hole
•OH	Hydroxyl Radical
SD	Standard Deviation
HSD	Honest Significant Difference
F	F-statistic (the ratio of variances used in ANOVA to test the overall significance)

Term / Symbol	Definition / Meaning
Root MSE	Root Mean Square Error
α	Alpha level (the significance level, typically 0.05, used as a threshold for determining statistical significance)
n	Sample size (number of replicates or independent observations)
p	p-value (the probability that the observed results occurred by chance; indicates statistical significance)
C_0	Initial Concentration
C_t	Concentration at time t
pH	Potential of Hydrogen (acidity/basicity)
TDS	Total Dissolved Solids
CB	Conduction Band
VB	Valence Band
E_{VB}	Valence Band Energy
E_{CB}	Conduction Band Energy
NHE	Normal Hydrogen Electrode
TMOs	Transition Metal Oxides
LED	Light Emitting Diode
rpm	Revolutions Per Minute
hν	Photon Energy
E_g	Band Gap Energy
F(R)	Kubelka-Munk Function

Table S2. Yield of CuO–Cu_2O–Cu heterostructures obtained via solid-state reduction of 1.0 g CuO with different ascorbic acid masses

Sample ID	CuO (g)	Ascorbic acid (g)	Product mass (g) (Run 1/2/3)	Yield (%) (Run 1/2/3)
CuO–A0.2	1	0.2	0.91 /0.93 /0.915	91 /93 /91.1
CuO–A0.5	1	0.5	0.96 /0.968/ 0.954	96/ 96.8 /95.4
CuO–A0.8	1	0.8	0.962 /0.975 /0.97	96.2/ 97.5/ 97
CuO–A1.1	1	1.1	0.981 /0.99/0.97	98.1/ 99/ 97

Table S3. Raw experimental data for Cr(VI) photoreduction under different conditions (n = 3 replicates per condition).

Series	Condition	Run 1	Run 2	Run 3	±SD	Mean (%)
Concentration (mg L^{-1})	15	100	100	99.91	0.05	99.97
	25	100	100	99.4	0.35	99.80
	35	97.43	94.43	99.60	2.60	97.15
	45	77.04	74.00	80.00	3.00	77.01
pH	2.5	100	97	100	1.73	99.00
	3.5	81.27	78	84	3.00	81.09
	5.8	31	28	34	3.00	31.00
	8	24.74	25	24	0.52	24.58
Catalyst Dosage (mg)	20	100	97	100	1.73	99.00
	30	100	100	99.4	0.35	99.80
	50	99.02	98.5	99.5	0.50	99.01

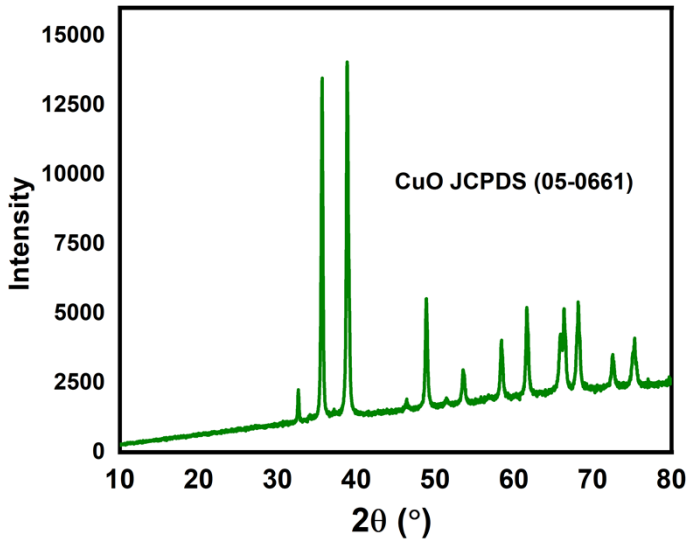

Fig. S1. XRD pattern of the control CuO sample calcined at 350 °C for 1 h in a covered crucible without ascorbic acid.

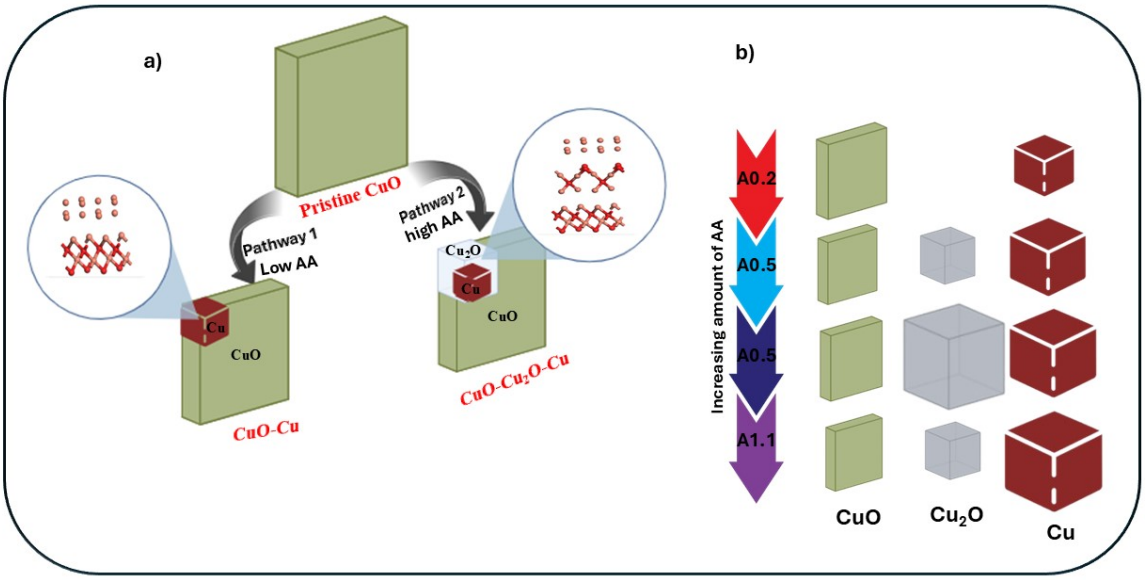

Scheme S1 Evolution of phase-specific crystallite sizes in Cu–Cu_2O–CuO heterostructures calculated from the Scherrer equation (a), and stepwise formation of Cu–Cu_2O–CuO heterostructures via sequential reduction of CuO by ascorbic acid (b).

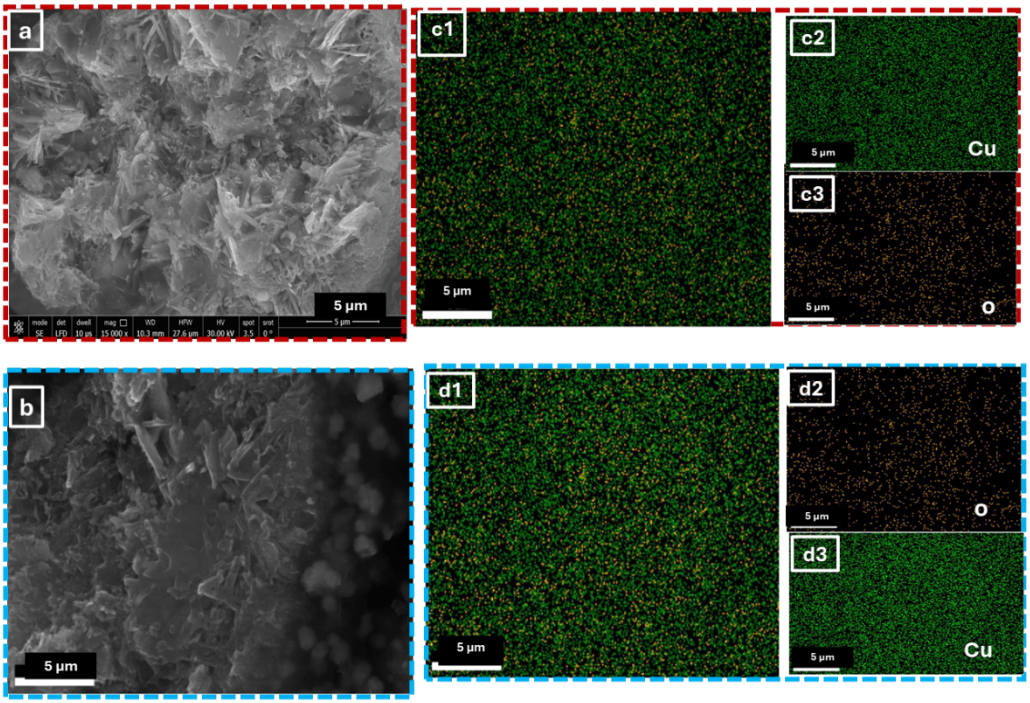

Fig. S2. SEM images of (a) CuO-A0.5 at high magnifications with corresponding elemental mapping (c1–c3). SEM images of (b) CuO-A1.1 at high magnifications with elemental mapping (d1–d3).

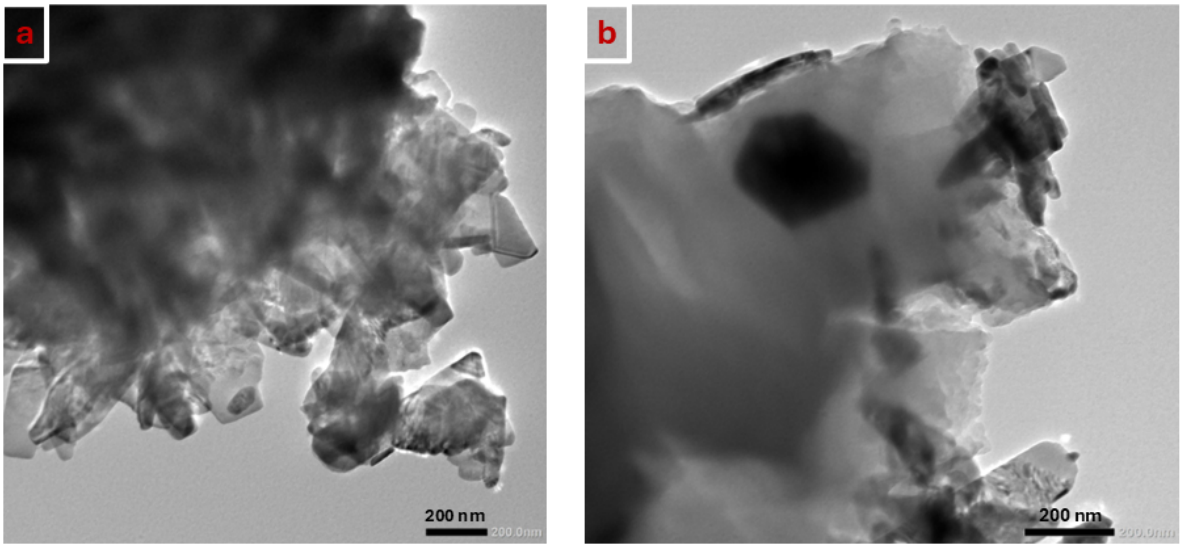

Fig. S3. TEM images of CuO-A0.5 (a) and CuO-A1.1 (b), at high magnifications.

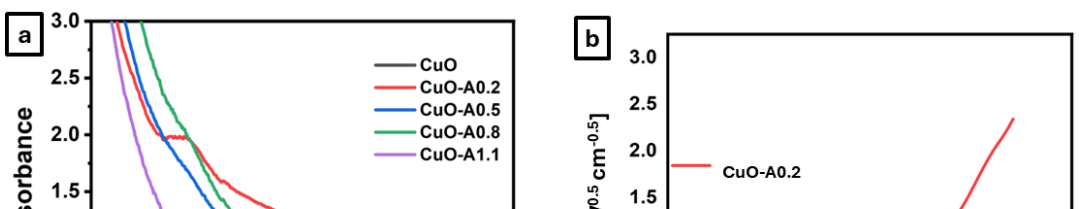

Fig. S4. UV–Vis absorption spectra (a), and Tauc plots for band gap estimation of CuO–Cu_2O–Cu heterostructure (b-d).

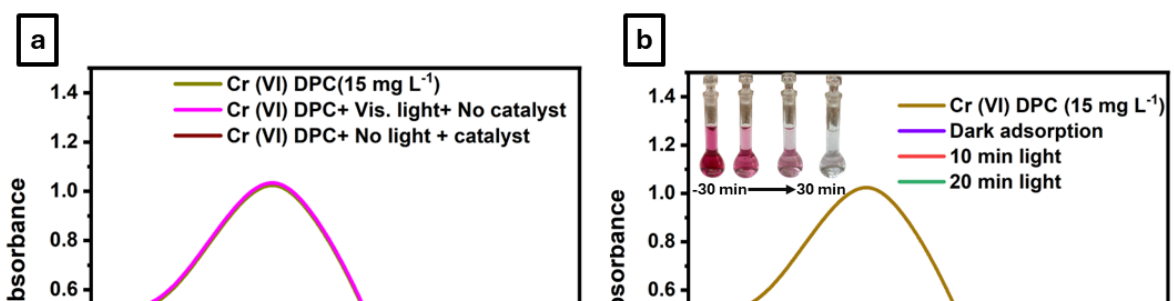

Fig. S5. Control experiments for Cr(VI) reduction: (a) without catalyst under visible light and with catalyst in the dark; (b) with the CuO–A1.1 catalyst under visible-light irradiation.

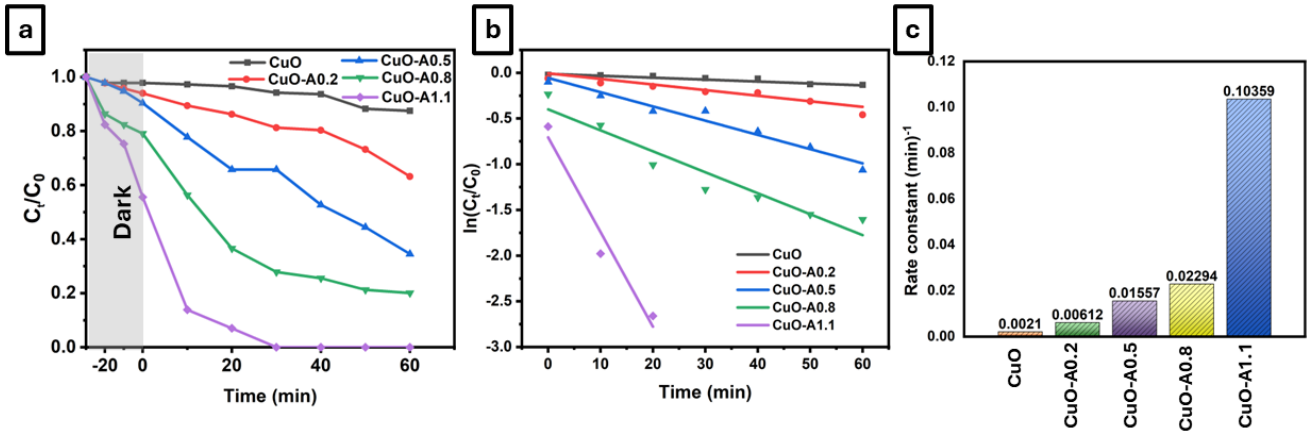

Fig. S6. Photocatalytic reduction of Cr(VI) under visible light irradiation: (a) performance of different CuO-Cu_2O-Cu catalysts, (b) pseudo-first-order kinetic plots, (c) apparent rate constants. (Cr(VI) concentration: 25 mg L^{-1}; catalyst dosage: 20 mg; PH 2.5; all tests performed in the presence of methanol).

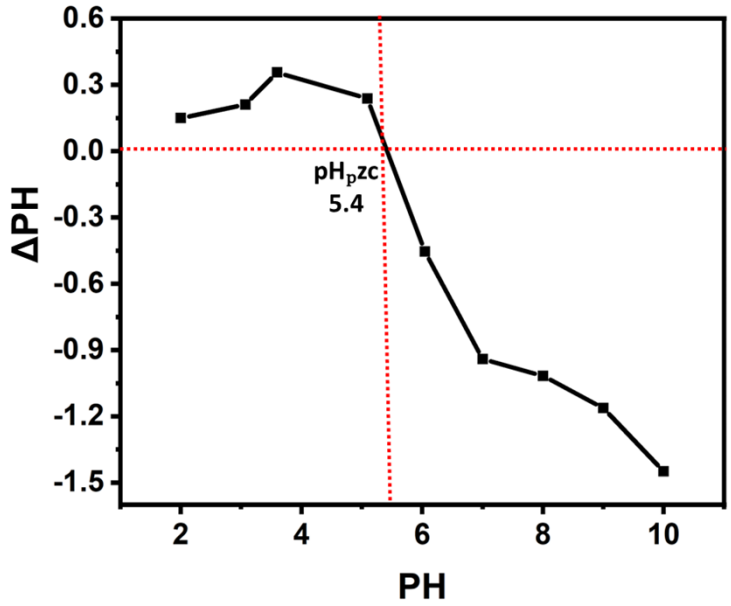

Fig. S7. Determination of the point of zero charge (pH_pzc) of CuO–A1.1 by the pH drift method.

Table S4. Descriptive statistics for Cr(VI) photoreduction under varying Cr(VI) concentrations, pH values, and catalyst dosages.

Conc (mg L^{-1})	N Analysis	N Missing	Mean	Standard Deviation	SE of Mean
15	3	0	99.97	0.05196	0.03
25	3	0	99.8	0.34641	0.2
35	3	0	97.15267	2.59655	1.49912
45	3	0	77.013	3.00008	1.7321
PH	**N Analysis**	**N Missing**	**Mean**	**Standard Deviation**	**SE of Mean**
2.5	3	0	99	1.73205	1
3.5	3	0	81.08867	3.00393	1.73432
5.8	3	0	31	3	1.73205
8	3	0	24.58	0.51884	0.29956
Dosage (mg)	**N Analysis**	**N Missing**	**Mean**	**Standard Deviation**	**SE of Mean**
20	3	0	99	1.73205	1
30	3	0	99.8	0.34641	0.2
50	3	0	99.00667	0.50013	0.28875

Table S5. One-way ANOVA results for the effect of concentration, pH, and catalyst dosage on Cr(VI) photoreduction efficiency.

Conc (mg L^{-1})	**DF**	**Sum of Squares**	**Mean Square**	**F Value**	**Prob>F**
Model	3	1100.13902	366.71301	92.4567	1.50E-06
Error	8	31.73057	3.96632		
Total	11	1131.8696			
PH	**DF**	**Sum of Squares**	**Mean Square**	**F Value**	**Prob>F**
Model	3	12169.85445	4056.61815	762.06435	3.63E-10
Error	8	42.58557	5.3232		
Total	11	12212.44002			
Dosage (mg)	**DF**	**Sum of Squares**	**Mean Square**	**F Value**	**Prob>F**
Model	2	1.26942	0.63471	0.565	0.59591
Error	6	6.74027	1.12338		
Total	8	8.00969			

Table S6. Fit Statistics for One-way ANOVA results for the effect of concentration, pH, and catalyst dosage on Cr(VI) photoreduction efficiency.

	PH	**Conc. (mg L^{-1})**	**Dosage (mg)**
R-Square	0.99651	0.97197	0.15849
Coeff Var	0.03916	0.0213	0.01068
Root MSE	2.30721	1.99156	1.0599
Data Mean	58.91717	93.48392	99.26889

Table S7. Tukey's HSD pairwise comparison test for mean differences between factor levels.

Conc (mg L^{-1})	MeanDiff	SEM	q Value	Prob	Alpha	Sig	LCL	UCL
25 - 15	-0.17	1.63	0.15	1.00	0.05	0.00	-5.38	5.04
35 - 15	-2.82	1.63	2.45	0.37	0.05	0.00	-8.02	2.39
35 - 25	-2.65	1.63	2.30	0.42	0.05	0.00	-7.85	2.56
45 - 15	-22.96	1.63	19.97	0.00	0.05	1.00	-28.16	-17.75
45 - 25	-22.79	1.63	19.82	0.00	0.05	1.00	-27.99	-17.58
45 - 35	-20.14	1.63	17.52	0.00	0.05	1.00	-25.35	-14.93
PH	**MeanDiff**	**SEM**	**q Value**	**Prob**	**Alpha**	**Sig**	**LCL**	**UCL**
3.5 - 2.5	-17.91	1.88	13.45	0.00	0.05	1.00	-23.94	-11.88
5.8 - 2.5	-68.00	1.88	51.05	0.00	0.05	1.00	-74.03	-61.97
5.8 - 3.5	-50.09	1.88	37.60	0.00	0.05	1.00	-56.12	-44.06
8 - 2.5	-74.42	1.88	55.87	0.00	0.05	1.00	-80.45	-68.39
8 - 3.5	-56.51	1.88	42.42	0.00	0.05	1.00	-62.54	-50.48
8 - 5.8	-6.42	1.88	4.82	0.04	0.05	1.00	-12.45	-0.39
Dosage (mg)	**MeanDiff**	**SEM**	**q Value**	**Prob**	**Alpha**	**Sig**	**LCL**	**UCL**
30 - 20	0.80	0.87	1.31	0.65	0.05	0.00	-1.86	3.46
50 - 20	0.01	0.87	0.01	1.00	0.05	0.00	-2.65	2.66
50 - 30	-0.79	0.87	1.30	0.65	0.05	0.00	-3.45	1.86

Table S8. Results of Levene's test for homogeneity of variances for the photoreduction efficiency data under different experimental conditions.

PH	DF	Sum of Squares	Mean Square	F Value	Prob>F
Model	3	5.45309	1.8177	1.20338	0.36894
Error	8	12.08389	1.51049		
Conc. (mg L^{-1})	**DF**	**Sum of Squares**	**Mean Square**	**F Value**	**Prob>F**
Model	3	9.41395	3.13798	2.63777	0.12126
Error	8	9.51707	1.18963		
Dosage (mg)	**DF**	**Sum of Squares**	**Mean Square**	**F Value**	**Prob>F**
Model	2	2.13397	1.06698	7.51998	0.02319
Error	6	0.85132	0.14189		

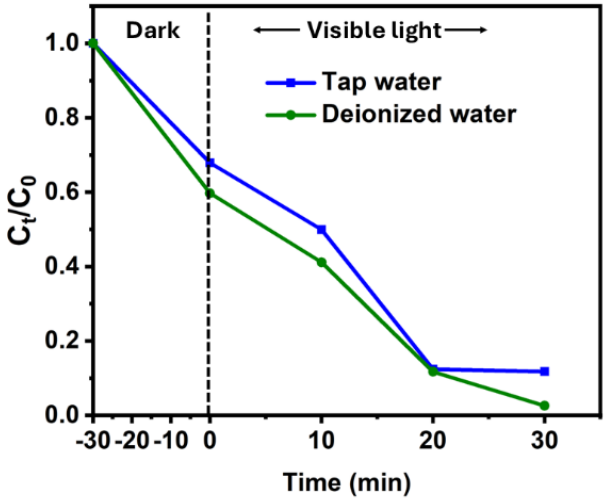

Fig. S8. Photocatalytic reduction of Cr(VI) in tap water using the CuO–A1.1. The tests were conducted in Cr(VI)-spiked tap water (conductivity = 290–350 µS cm^{-1}, TDS = 191–231 ppm) containing common ions .g., (Cl^-, SO_4^{2-}, HCO_3^-). Under identical experimental conditions to the deionized-water system (Cr(VI) = 35 mg L^{-1}, catalyst dose = 0.02 g, pH = 2.5, 40 mL).

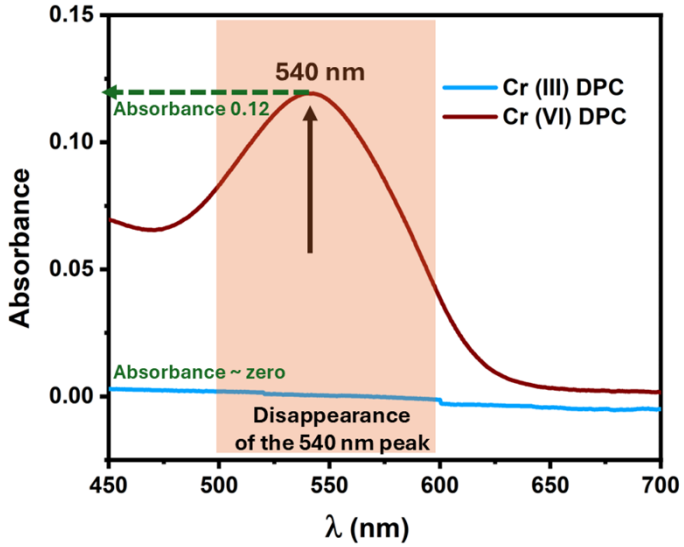

Fig. S9. UV–Vis spectra of Cr(VI)–DPC (540 nm) and Cr(III)–DPC, confirming photocatalytic reduction of Cr(VI) to Cr(III).

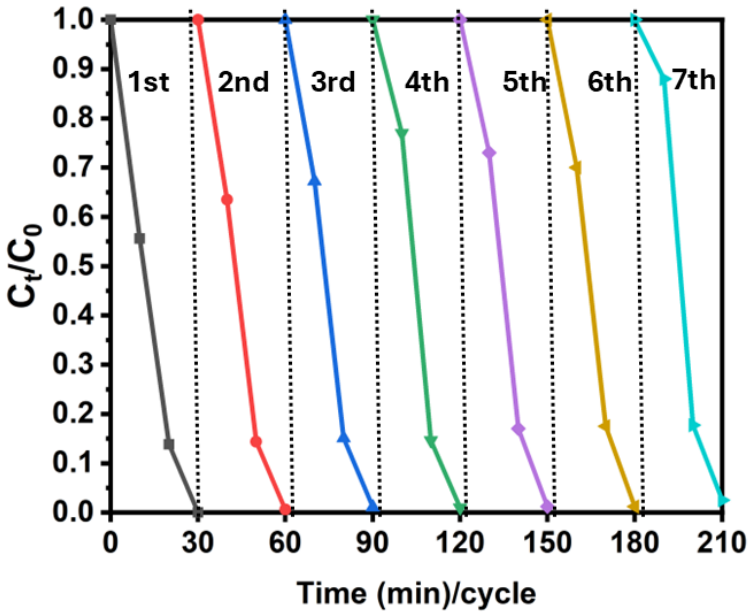

Fig. S10. Concentration profiles (C_t/C_0 vs. time) for 7 consecutive photocatalytic cycles using the CuO–A1.1.

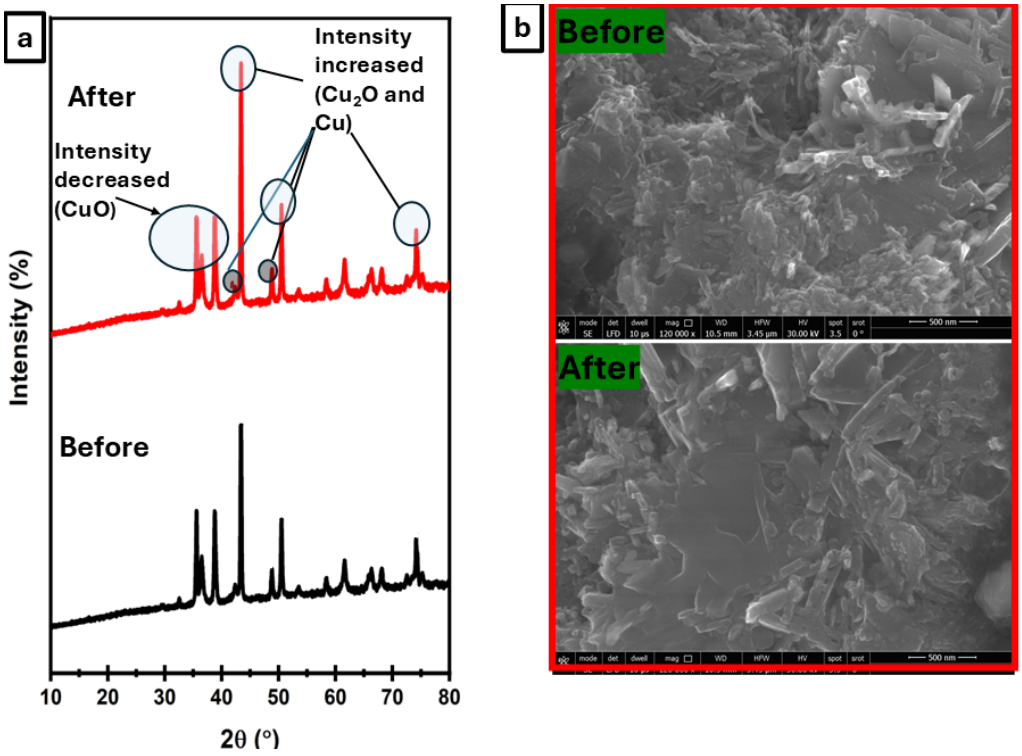

Fig. S11. Post-photocatalysis characterization of CuO-A1.1: XRD patterns (a), and SEM analysis (b).